Harnessing Selectivity and Sensitivity in Ion Sensing via Supramolecular Recognition: a 3D Hybrid Gold Nanoparticle Network Chemiresistor

Verónica Montes-García, Rafael Furlan de Oliveira, Ye Wang, Andrey Berezin, Pablo Fanjul-Bolado, María Begoña González García, Thomas M. Hermans, Davide Bonifazi, Stefano Casalini,* and Paolo Samorì**

Dr. V. Montes-García, Dr. R. Furlan de Oliveira, Y. Wang, Dr. T. M. Hermans, Dr. S. Casalini, Prof. P. Samorì
University of Strasbourg, CNRS, ISIS UMR 7006, 8 Alleé Gaspard Monge, F-67000 Strasbourg, France.
E-mail: samori@unistra.fr

Dr. A. Berezin, Prof. D. Bonifazi
School of Chemistry, Cardiff University, Park Place, CF10 3AT, Cardiff, United Kingdom

Dr. P. Fanjul-Bolado, Dr. M. B. González García
Metrohm DropSens S.L. Vivario de Ciencias de la Salud, Calle Colegio Santo Domingo de Guzmán, 33010, Oviedo, Asturias, Spain

Dr. T. M. Hermans
Université de Strasbourg, CNRS, UMR 7140, 4 Rue Blaise Pascal, 67081 Strasbourg, France

Prof. D. Bonifazi
Institute of Organic Chemistry, University of Vienna, 1090 Vienna, Austria.
E-mail: davide.bonifazi@univie.ac.at

Dr. S. Casalini
Current address: Università degli Studi di Padova, Dipartimento di Scienze Chimiche, via Marzolo 1, 35131 Padova, Italy.
E-mail: stefano.casalini@unipd.it

Keywords: Chemiresistors, metal nanoparticles, point-of-care sensor, microfluidics, molecular recognition

The monitoring of K^+ in saliva, blood, urine, or sweat represents a future powerful alternative diagnostic tool to prevent various diseases. However, several K^+ sensors are unable to meet the requirements for the development of point-of-care (POC) sensors. To tackle this grand-challenge, here we report the fabrication of chemiresistors (CRs) based on 3D networks of Au nanoparticle (AuNP) covalently bridged by ad-hoc supramolecular receptors for K^+, namely dithiomethylene dibenzo-18-crown-6 ether. A multi-technique characterization allowed us to optimize a new protocol for fabricating high-performing CRs for real-time monitoring of K^+ in complex aqueous environments. Our sensor shows exceptional figures of merit: i) linear

sensitivity in the 10^{-3} M to 10^{-6} M concentration range; ii) high selectivity to K^+ in presence of interfering cations (Na^+, Ca^{2+}, and Mg^{2+}); iii) high shelf-life stability (>45 days); iv) reversibility of K^+ binding and release; v) successful device integration into microfluidic systems for real-time monitoring; vi) fast response and recovery times (<18 s), and v) K^+ detection in artificial saliva. All these characteristics make our supramolecular CRs a potential tool for future application as POC devices, especially for health monitoring where the determination of K^+ in saliva is pivotal for the early diagnosis of diseases.

1. Introduction

The Potassium cation (K^+) is one of the most abundant physiological metal ions in living organisms, playing vital roles in many biological processes, such as blood pressure control, digestion, nerve conduction, regulation of muscle contractions, osmoregulation, heartbeat, etc.[1] K^+ is ubiquitous, being found in all common bodily fluids including saliva, sweat, and blood, in a typical concentration of 3.5-5.5 mmol/L (137-215 mg/L).[2] Unfortunately, K^+ homeostasis is affected by the intake of medication, the presence of other ions, or bad alimentary habits.[3] Both, high levels of K^+ (hyperkalaemia) and low levels of K^+ (hypokalaemeia) may result from disruptions in transcellular homeostasis or in the renal regulation of potassium excretion.

In this context, the development of effective methods to detect K^+ is urgently needed, being crucial for the early detection of related diseases. Different standard analytical methods are commonly exploited including flame photometry,[4] atomic absorption/emission spectrophotometry,[5] or ion chromatography.[6] Other, novel K^+ sensing technologies have been developed recently, like ion-selective electrodes,[7] fluorescent,[8] colorimetric,[9], and electrochemical sensors [10]. Although some of them feature high sensitivity and selectivity, these methods do not show a well-balanced combination of characteristics to afford their practical application in our daily lives as point-of-care (POC) sensors. Chemiresistors (CRs)

[11] are a compelling alternative which possess considerable advantages for POC applications, including excellent sensitivity, cost-effectiveness, simple sensing mechanism,[12] portability,[13] facile integration into microfluidic systems[14] and combination with optoelectronic transducers.[15]

Noble metal nanoparticles (NPs) are ideal scaffolds for the fabrication of different types of sensing devices,[16] especially CRs,[12, 17] due to their high surface-to-volume ratio and unique optical and electrical properties, which are very sensitive to chemical events occurring in their surroundings. According to the Kubo model,[18] Au NPs having a diameter exceeding ca. 2 nm behave as nanoscopic electrical conductors obeying Ohm's law.[18] Even though the development of CRs dates back to 1985,[19] the implementation of noble metal NPs as sensing material in CRs is more recent, especially for sensing directly into liquid media. In such devices, specific organic molecules are employed in order to form a robust network of NPs, whose electrical features can be modulated by the analyte physical absorption and release. [20]

Wohljen and Snow developed the first NP-based CR for vapor sensing.[11a] They fabricated a device featuring a film of octanethiol-capped Au NPs on interdigitated electrodes (IDEs) that was exposed to various volatile compounds such as toluene, tetrachloroethene, 1-propanol, and water vapor. Variations of the electrical resistance of the device were ascribed to the interaction of the volatile molecules with the NP network, which undergoes swelling, producing structural changes. [11a] The same rationale has been successfully demonstrated by using specific CRs operating in liquid, whose geometrical layout is designed to minimize electrical contributions arising from the electrolytic solution.[21] As a result, Raguse and co-workers reported the first CR based on a thin film of Au NPs capped with 1-hexanethiol monolayer inkjet-printed onto a microelectrode.[21] This sensor featured very interesting properties such as fast response time (< 3 min) and high sensitivity (down to the 0.1 ppm range) towards toluene, dichloromethane, and ethanol molecules dissolved in 1 M KCl solutions.[21] Since then, many efforts have been

devoted to the optimization of the sensing performance of CRs. The supramolecular interaction between analytes and receptors[22] followed by alterations of the electron transport through metal NP networks [23] acting as signal transduction, are two fundamental phenomena that make CRs extremely sensitive device for chemical sensing. To the best of our knowledge, few examples of CRs based on metal NPs for ion sensing (viz. Cu^{2+},[24] and Zn^{2+}, Cd^{2+}, and CH_3Hg^+) have been published so far.[25] However, these devices rely on the strong complex formation between the receptor and the cations of interest operating in dry state. Such a technology satisfies the demand for single-use (*i.e.*, disposable) sensors, but it cannot provide a sound option for continuous, real-time monitoring of the analyte of interest. To fill this gap, we report on the fabrication of metal NP-based CRs capable to perform real-time and selective sensing of K^+ in water and in complex matrices, such as artificial saliva, driven by supramolecular interactions.[26] Crown ethers, which are well-known macrocycles able to complex ions via reversible host-guest interactions [27], bearing two peripheral thiol groups were devised to conceive a 3D covalently-linked network of AuNPs. Here, dibenzo-18-crown-6 (DTDB-18C6) molecules act as both linkers to build up the 3D AuNP networks and supramolecular K^+ receptors.[28] The network fabrication is achieved by an iterative deposition of Au NPs and DTDB-18C6 molecules through covalent layer-by-layer (LbL) assembly technique onto a glass substrate featuring IDEs on top. We built up a standardized deposition protocol of these two components in order to precisely control the network assembly by evaluating important parameters such as the Au NPs size, adhesive layers, and deposition kinetics. The CR performance was studied and optimized in terms of number of deposition steps for network formation, NPs size, as well as the IDEs layout. The selectivity of the sensing platform towards K^+ was analysed in the presence of the most common interfering metal cations present in bodily fluids (Na^+, Ca^{2+}, and Mg^{2+}). We have also performed the monitoring of K^+ in water by means of a microfluidic system aiming for the development of a PoC technology able to provide real-time responses. Finally, we challenged the sensing performance of our CR

in artificial saliva in order to verify its effective sensitivity and selectivity in complex media. The successful K^+ detection in saliva endows such a CR the required characteristics to be used as the sensing element in future technologies for alternative health monitoring and early diagnostics of diseases.

2. Results and Discussion

2.1. Chemiresistor Fabrication and Operation

The assembly of the 3D covalent network for the fabrication of CRs relies on two key components: i) citrate-stabilized Au NPs [29] (Figures S1-2), and ii) a dithiomethylene dibenzo-18-crown-6 ether, DTDB-18C6 (Scheme S1, Figures S3-7). The former endows the sensing platform with excellent electrical features for signal transduction,[11b] whereas the latter guarantees the covalent linkage of adjacent Au NPs and the supramolecular recognition of K^+ via well-known host−guest interactions. [27-28]

The fabrication of the CRs has been the subject of a deep investigation in order to optimize its overall sensing performance. The final protocol consisted of 4 steps: i) substrate cleaning, ii) deposition of an adhesive layer for Au NP attachment, iii) Au NPs deposition, and iv) DTDB-18C6 grafting. The first two steps have been adapted from previous protocols.[30] Aiming at a standardized deposition of Au NPs the choice of the adhesive layer is pivotal, as its chemical features must provide both strong adhesion of Au NPs on the substrate surface and precise control over their spacing for molecular bridging with DTBB-18C6 linkers. As mentioned in the experimental section, four approaches have been explored such as no adhesive layer, dithiolated TEG, PDDA, and APTES (Figure S8). No adhesion (Figure S8a), partial adhesion (Figure S8b), and uncontrolled grafting (Figure S8c) of Au NPs have been observed respectively by making use of the first three approaches. The best option turned out to be APTES (Figure S8d), which allowed a controlled deposition of Au NPs over the entire chip that is composed of a glass surface and Au IDEs. Although such a protocol guarantees a high control

upon the first deposited layer of Au NPs, two further aspects have been investigated in order to reach the best sensing performance, namely the UV/Ozone surface treatment during substrate cleaning and the purification or not of the Au NPs (Figure S9). The former turned out to be detrimental for K^+ sensing because it creates negative charges on the substrate capable to interfere with the supramolecular interaction exerted by DTDB-18C6 (Figure S9a). The latter filters out the excess Na^+ cations and citrate anions in the Au NP solution. We observed that no purification leads to higher controlled substrate coverage, as the high ionic strength of the Au NP solution is responsible to keep the NPs closer with respect to a purified solution in bi-distilled water (Figure S9b). Thus, the optimized conditions rely on APTES as an adhesive layer, no UV/ozone substrate treatment, and no previous purification of Au NPs.

The 3D AuNP-DTDB-18C6 network was assembled onto glass chips by the LbL approach (**Figure 1a**) that can be summarized as (i) APTES adhesive layer deposition onto glass substrate *via* immersion into a 1% v/v aqueous dispersion of APTES, (ii) Au NPs covalently attachment *via* immersion of the modified substrate into an aqueous dispersion of 0.5 mM Au NPs, (iii) DTDB-18C6 macrocycles covalently grafted on the surface of Au NPs *via* immersion in a 1 mM DTDB-18C6 DMF solution. The iteration of step ii and iii defines the number of deposition steps (DSs) for the network formation. Hereafter, one DS means the ensemble of step ii and step iii.

Concerning the CR operation and signal transduction, electrical impedance spectroscopy (EIS) has been chosen to ensure high sensitivity and avoid electrophoretic effects exerted by a standard DC bias, insofar reducing electrical drift and enhancing the reversibility of the sensor response.[21, 31] Impedance measurements provide many parameters that can be used as the output signal in a sensing device, such as the impedance module (Z), imaginary (Z'') and real (Z') parts of impedance, capacitance (C), and impedance phase (ϕ).[21, 32] Our investigation is mainly focused on capacitive changes, where the CR's output signal (Cp) is obtained from equation (see details in the *Supporting Information*):

$$C_P = \frac{-Z''}{2 \cdot \pi \cdot \nu \cdot |Z|^2}$$ Equation (1)

where ν is the frequency of the AC stimulus.

Our rationale is similar to the one introduced by Raguse *et al.* who employed single-pair electrodes to measure the impedance response of functionalized Au NPs to the presence of organic analytes in water.[21] Here, we use an IDEs layout to maximize the sensor active area, allowing us to exploit the capacitance changes in the network due to K^+ intake and supramolecular recognition by the macrocyclic host. For this purpose, we initially identified the most appropriate CR operational frequencies by comparing the response of the bare and the network-coated IDEs in a series of K^+ solutions with concentration spanning from 10^{-6} to 10^{-1} M (Figure S11). From the capacitance (Cp)-frequency response of the network-coated IDE, we observed that 0.1 Hz is the best frequency, where Cp increases by 443% in 10^{-3} M K^+, distinctively from Cp increase in water (283%) and the response of the bare chip (**Figures 1b** and **1c**). Indeed, at low frequencies (< 100 Hz) charged species in solution have enough time to follow the alternating electric field to interact non-covalently with the supramolecular receptors in the AuNP network, contributing to the overall capacitance increase of the device.[32] At high frequencies (10^5 Hz), K^+ ions are unable to follow the electric field oscillations, and the Cp corresponds to the geometric capacitance of the IDEs having the solution as the dielectric medium.[32] Other, intermediate frequencies were not able to provide undistinguishable output Cp responses for the K^+ detection at varying concentrations, as a result of the recognition mechanism (Figure S11). At such intermediate frequencies, the bare chips respond non-selectively to the increase of the K^+ concentration, very likely due to a corresponding increase of the electrolyte conductivity.

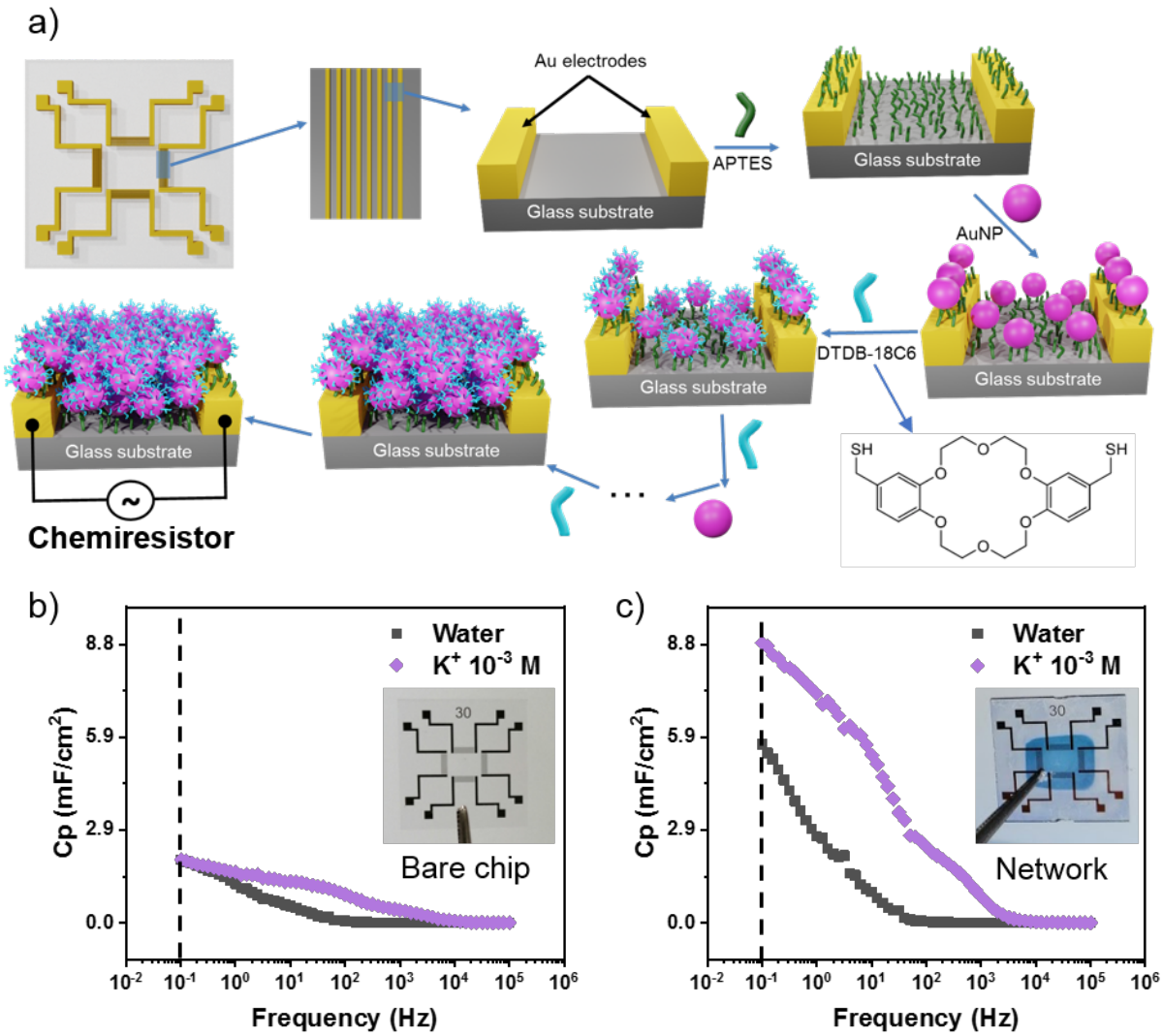

Figure 1: a) Schematic layer-by-layer fabrication of CRs based on covalently assembled AuNP-DTDB18C6 networks, b-c) Capacitance response of b) bare and c) Au NPs-DTDB18C6 network-coated IDEs in Milli Q water (black curves) and K^+ 10^{-3} M (violet curves). Inset: Respective pictures of the bare and network-coated glass chips.

2.2. Optimization of the CR sensing capabilities

The CR's sensing core is the 3D covalent network assembled onto the IDEs. The proper functioning of this platform relies on the accurate control of the deposited Au NPs and their bridging by DTDB-18C6 macrocycles. Thus, to optimize the CR performance, two key-

parameters have been assessed: i) the assembly kinetics of the network individual components (*viz.* AuNPs and DTDB-18C6), and ii) the number of DSs.

The kinetics has been characterized by monitoring the temporal evolution of Cp at 0.1 Hz for both of the individual network components (**Figure 2a**). In particular, it takes 40 min for the DTDB-18C6 molecules to displace completely the citrate anions of the solvation shell of Au NPs immobilized during the first DS (Figure S12). This process is pivotal for achieving reliable CR responses as citrate traces can act as unspecific sites capable to electrostatically compete against the supramolecular recognition of K^+ by the crown ether receptors, in addition to responding to several cationic interferents. The replacement of the negatively-charged citrate by DTDB-18C6 results in a decrease of Cp, likely ascribed to a decrease of the overall charges in the AuNPs immobilized in the network. The subsequent deposition of DTDB-18C6 showed faster kinetics (ca. 15 min) with respect to the initial one. On the other hand, Au NPs showed slower kinetics for any DS. Although a plateau is not reached, we defined 45 min as a reasonable immersion time for their deposition. Conversely to the DTDB-18C6 attachment, the grafting of Au NPs resulted in a clear increase of Cp, which can be ascribed to the formation of a 3D network endowed of larger active area and volume, along with the contribution of excess charges from stabilizing citrate molecules.

Concerning the number of DSs, we monitored the electrical resistance of the networks in dry state for DSs varying from 1 to 11. The measured the CR's resistance (R) and corresponding DSs can be grouped in three regions: i) few DSs (>10 GΩ), ii) 5-6 DSs (2-5 GΩ), and 11 DSs (< 1 GΩ), as shown in **Figure 2b**. Such a less resistive trend is consistent with the improved surface coverage by the 3D covalent network onto the IDEs, as revealed by SEM images (Figure S13). For DSs equal to 1, 3, 6, and 11, we found surface coverages of 29.60%, 36.49%, 47.79% and 85.89%, respectively. The higher the coverage, the more parallel paths for charge transport are created within the network, thereby decreasing the overall electrical resistance. The increase of the number of DSs is followed by a coherent increase of Cp, both in pure water and in a K^+

10^{-3} M solution, due to the formation of a 3D network endowed of larger area and volume (**Figure 2c**).

In order to evaluate the CR sensing capabilities, networks formed by 6 and 11 DSs have been tested (**Figure 2d**). As previously discussed, networks composed by only a few DSs possess poor substrate coverage, which compromise the ultimate CR sensing performance. Both tested networks (viz. 6 and 11 DSs) exhibited similar sensitivity (S) towards K^+ within the mM-μM concentration range (i.e. 10^{-3}-10^{-6} M), as shown in **Figure 2d**. As the increase of the DSs does not reflect in a substantial gain of sensitivity or detectable K^+ concentration range, further sensing experiments were performed with CRs bearing networks formed by 6 DSs rather than 11 that are more time consuming (10 vs. 15 h for their respective fabrication). Within this context, other parameters governing the CR performance were also evaluated, including the IDEs geometry (i.e. electrodes spacing of 10, 20 and 30 μm) and Au NP size (namely, ∅ equal to 12.5, 24, and 40 nm), as shown in Figures S14a and S14b, respectively. Minor changes have been observed while varying such a wide combination of parameters, hence IDEs bearing electrodes with 30 μm spacing along with 12.5 nm Au NPs have been selected the final CR configuration for optimal sensing performance.

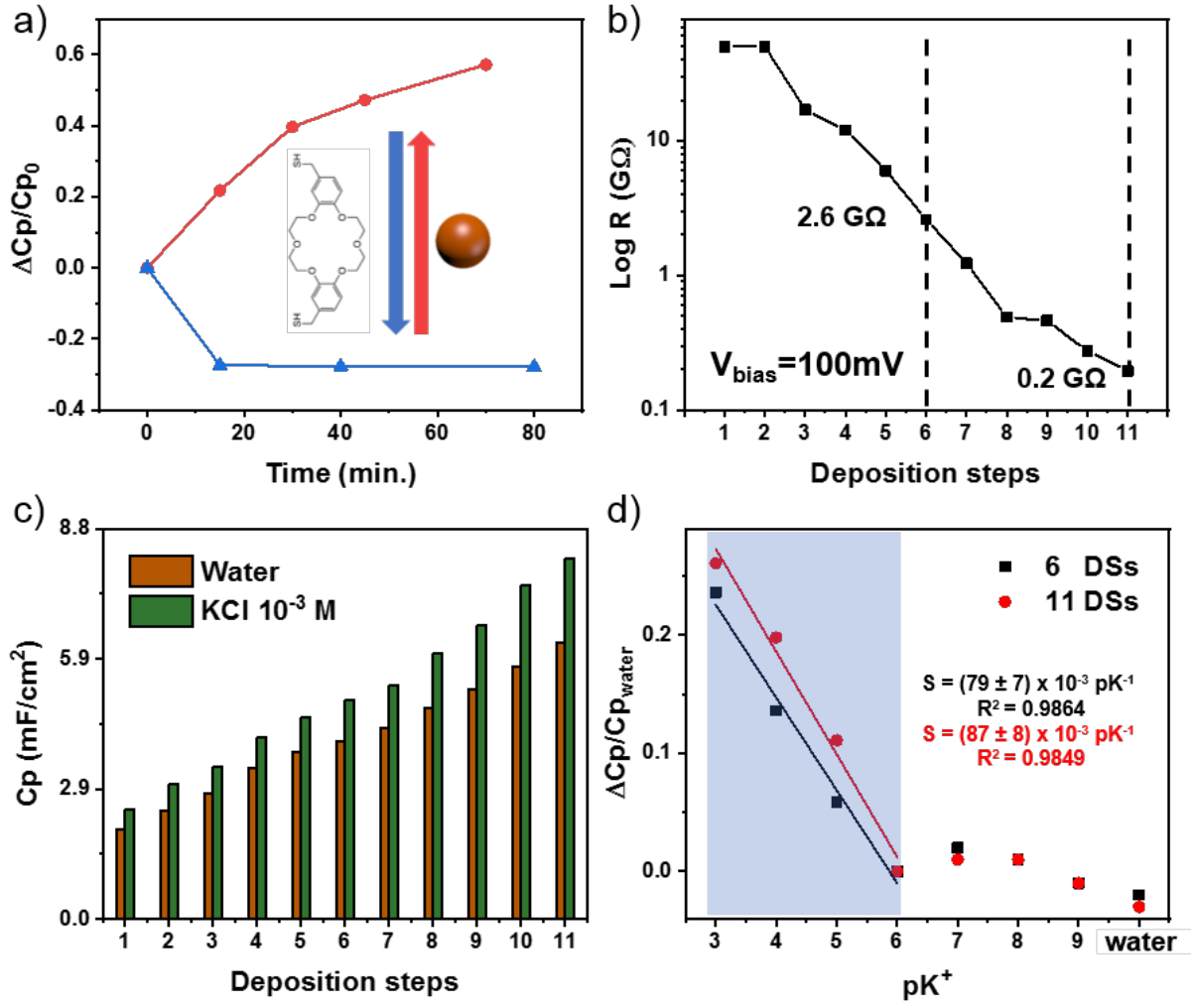

Figure 2: a) Kinetics plot (normalized Cp variations vs. immersion time) for the deposition of Au NPs (red curve) and DTDB-18C6 molecules (blue curve), recorded at 0.1 Hz in water; b) electrical resistance (R) and c) capacitance (Cp) as a function of the AuNPs-DB18C6 network DSs. Resistance measurements were performed in air, while capacitance measurements were carried out in both water and K^+ 10^{-3} M solution; d) Normalized capacitance response ($\Delta Cp/Cp_{water}$) as a function of the K^+ concentration for CRs based on AuNPs-DB18C6 networks formed by 6 (black curve) and 11 (red curve) DSs.

2.3. Device Sensing Performance

Several relevant aspects related to the CR performance have been investigated, such as the best EIS-related output signal, its pH-dependency and reversibility, the device stability and shelf-

life, and also the underlying sensing mechanism. Such investigations have been accomplished by impedance spectroscopy, optical spectroscopy, SEM, and XPS.

From the different parameters obtained by EIS measurements, such as the impedance modulus (Z), the impedance imaginary (Z'') and real parts (Z'), conductance (G_p), impedance phase (ϕ), capacitance (Cp), etc., we verified that the low-frequency Cp is the one presenting the most sensitive and straightforward CR signal translation of the selective detection of K^+ at different concentrations (Figures S15 and S16). Low-frequency Cp changes are related to the ability of cations to follow the oscillations of the electric field,[32] thereby interacting with the supramolecular receptors within the network. From the Cp output signal, a sensitivity of 0.075 pK^{-1} featuring a linear response within a K^+ concentration range of 10^{-3} to 10^{-6} M with a correlation coefficient of $R^2 = 0.9845$ (**Figure 3a**).

For sensing applications in real bodily fluids (*e.g.*, saliva, sweat, blood, to name a few), it is important to obtain a stable CR response upon media subjected to pH variations. **Figure 3b** shows that the CR response (Cp) varies to a maximum of 10% for measurements carried out in K^+ 10^{-3} M for pH spanning from 3.5 to 11. This indicates that our CRs do not need any support of a buffer solution to give a reliable response, and practical applications can rely on a simple calibration procedure according to the medium's pH.

The stability and reversibility of the electrical signal are other two important aspects of real sensing applications. Here, we have monitored the continuous CR output signal in 10^{-3} M K^+ for more than 1 h. We found the maximum relative standard deviation (RSD) of 1.8% (Figure S17). Furthermore, the device was exposed to water and 10^{-3} K^+ repeatably in order to define the degree of signal reversibility related to cation recognition (**Figure 3c**). The data were acquired after 1 min of the CR immersion in the solution of interest and then rinsed by bi-distilled water. From **Figure 3c**, one can observe the complete reversibility of the CR output signal. Such an important outcome arises from the properties of our 3D covalent network based on Au NP and DTDB-18C6 where K^+ detection is endowed by non-covalent host-guest

interactions. This hints that this technology overcomes the usual limitation of single-shot sensors. [7, 9a]

Shelf-life is another prerequisite for of the development of robust sensing technologies. Aiming at assessing the stability of our CRs, we compared the response of devices stored in air and in water. We monitored the CR resistance in dry state and Cp in water (Figure S18). As previously mentioned, dithiolated DTDB-18C6 molecules are handled in an O_2-free condition for the network assembly to avoid the formation of polymeric disulfides.[33] For this reason, CRs stored in air showed a marked instability when compared to those kept in water, which can be ascribed to the different oxygen content in the two environments (viz. dissolved oxygen in air and in water correspond to 21% and 1%, respectively). This rationale is supported by XPS data (Figure S19), which reveal a dramatic increase of the physically adsorbed sulphur with respect to covalently bonded one for devices stored in air. This is accompanied by the appearance of a new peak at 169 eV related to the SO_4^{2-} bond and hence to the oxidized sulfur. On the contrary, the stability of Au NPs is not affected by the different types of storage, as also verified by XPS (Figure S19a,c). Within 45 days of storage in water (data not shown), the CR resistance and capacitance varied less than 1.4% each.

As aforementioned, the sensing mechanism is expected to be governed by the reversible adsorption/desorption of K^+ occurring with the supramolecular recognition moieties of the AuNPs-DTDB-18C6 network. Such an interaction could modify the network's structure (*e.g.*, via swelling), changing its electrical properties. Thus, variations of the CR output signal would be ascribed to such structural modifications rather than the recognition action by the receptor molecules. To investigate a possible swelling, we evaluated the optical properties of the AuNPs-DTDB-18C6 network during the host-guest pairing by immersing the device in pure water and in K^+ 10^{-3} M solution (Figure S20). The optical extinction spectrum of the 3D covalent network features a plasmon band at 516 nm related to the dipole resonance of individual Au NPs, as well as a broad band at 850 nm due to the plasmon coupling between NPs in close proximity.[34]

The network exposure to K^+ does not affect such optical features (*i.e.*, no wavelength shift), suggesting that swelling does not occur during the sensing event. This indicates a pure electronic effect resulting from the supramolecular interaction between K^+ and the 3D covalent network as the main mechanism at the basis of the sensor operation.

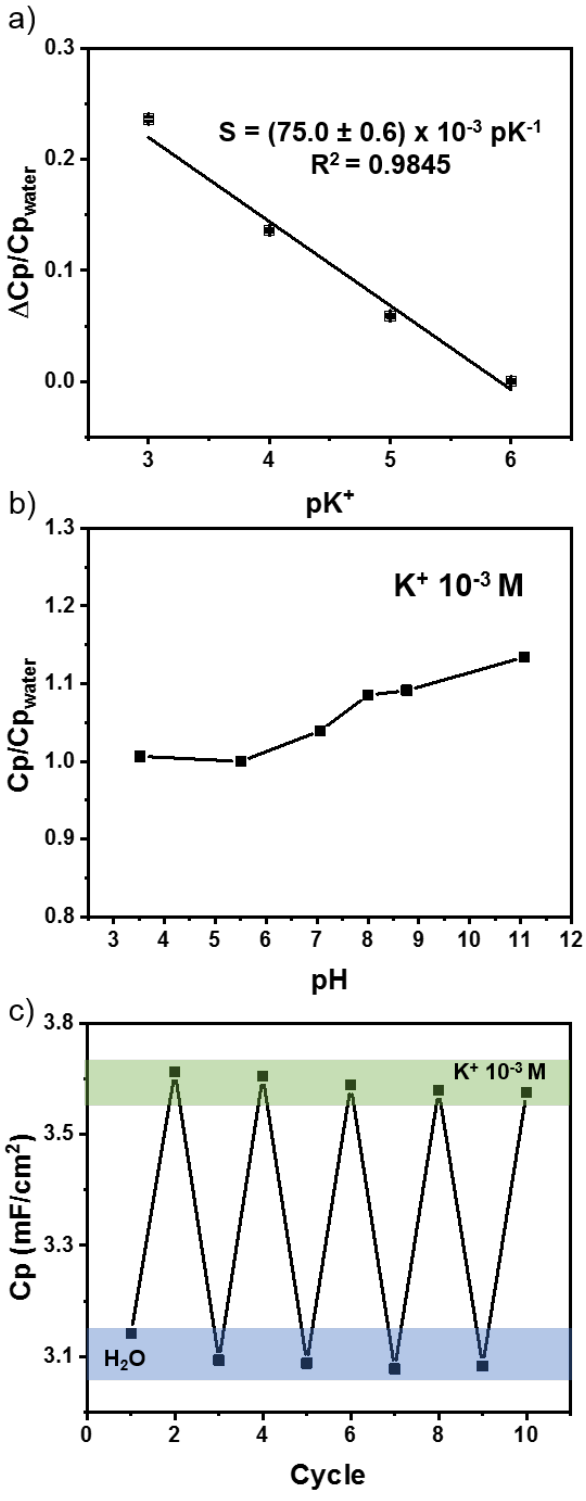

Figure 3: a) Normalized capacitance variation ($\Delta Cp/Cp_{water}$) as a function of K^+ concentration. b) capacitance response at K^+ 10^{-3} M as a function of pH; c) Reversible capacitance behaviour for the detection of K^+ 10^{-3} M. All the measurements were performed with CRs based on Au NPs-DTDB-18C6 networks having 6 DCs, with Cp recorded at 0.1 Hz.

2.4. Selectivity

Selectivity is one of the crucial figures of merit of a chemical sensor, hence the CR response towards Na^+, Ca^{2+}, and Mg^{2+} interferents at relevant concentrations has been tested. **Figures 4a** and **4b** illustrate the sensor response and respective sensitivities towards the different tested cations. The recorded device sensitivity is at least one order of magnitude higher for K^+ when compared to other tested cations. Our sensing experiments have been conceived by conditioning the device into the cation solution of interest for one min before performing the EIS measurements. Given the comparable, but slightly lower, affinity of crown ethers towards Na^+,[35] the CR response to the presence of Na^+ was registered for longer times to rule out the possibility of recognition events occurring at slower rates (Figure S21). No capacitive changes have been recorded on the timescale of ca. 1h, suggesting that no slow recognition processes compensating the lower affinity constant of DTDB-18C6 towards Na^+ occur. Provided that one min conditioning time is needed for reliable measurements (Figure S21), the outcome of these experiments not only prove the selectivity of our CRs, but it also validates our hypothesis for which these POC sensors can afford a fast-reliable response for practical applications like PoC sensing technologies.

The sensing mechanism of our CRs relies on the chemical affinity of the DTDB-18C6 receptor towards K^+ as a result of the match between the cation radius and the diameter of the crown ether cavity. To exclude that other non-covalent interactions govern the CR sensitivity and selectivity - such as any role played by Au NPs or peculiar characteristics of the chip as a result of its fabrication - we performed further investigations with reference systems. Devices bearing

as molecular receptors 1,10-decanedithiol and dithiolated TEG (Figure S22), whose contour length along the main molecular axis is similar to that of the DTDB-18C6 receptor (~16 Å), were thus engineered. The former linker lacks oxygen atoms in its structure, whereas the latter molecule (despite having oxygen atoms) does not possess a cage-like structure acting as a cation scavenger. The response of CRs based on networks formed by these two receptors, in addition to the bare device (i.e. in absence of active material in-between the IDEs), have been compared to the performance described by devices having networks bearing DTDB-18C6 receptors (**Figures 4c** and **4d**). Bare devices do not show any selectivity towards K^+, ruling out any unspecific interaction related to the chip characteristics (e.g. surface hydrophilicity) on the device response. CRs having 1,10-decanedithiol linkers showed a trend similar to the bare device, thereby highlighting the crucial role exerted by the molecule's oxygen atoms as a cation interaction site. Devices containing dithiolated TEG molecules showed some response towards K^+, however, a non-linear output signal as concentration increases was observed, in stark contrast to the linear response exhibited by DTDB-18C6 linkers over a broad K^+ concentration. Such a lack of linearity prevents us to determine the sensitivity of CRs made of dithiolated TEG receptors. More importantly these devices were found to respond similarly to other cations (viz. Na^+, Ca^{2+} and Mg^{2+}), displaying very limited selectivity (Figure S23). Slight differences in the intensity of the signal output though were found for mono- and bi-valent cations. These experiments not only point out the importance of having oxygen atoms in the molecular receptor for interactions with metal cations, but also the crown ether supramolecular cage structure and the 3D arrangement of such receptors in order to attain high cation selectivity and sensitivity by means of electrical transduction (Figure S24).

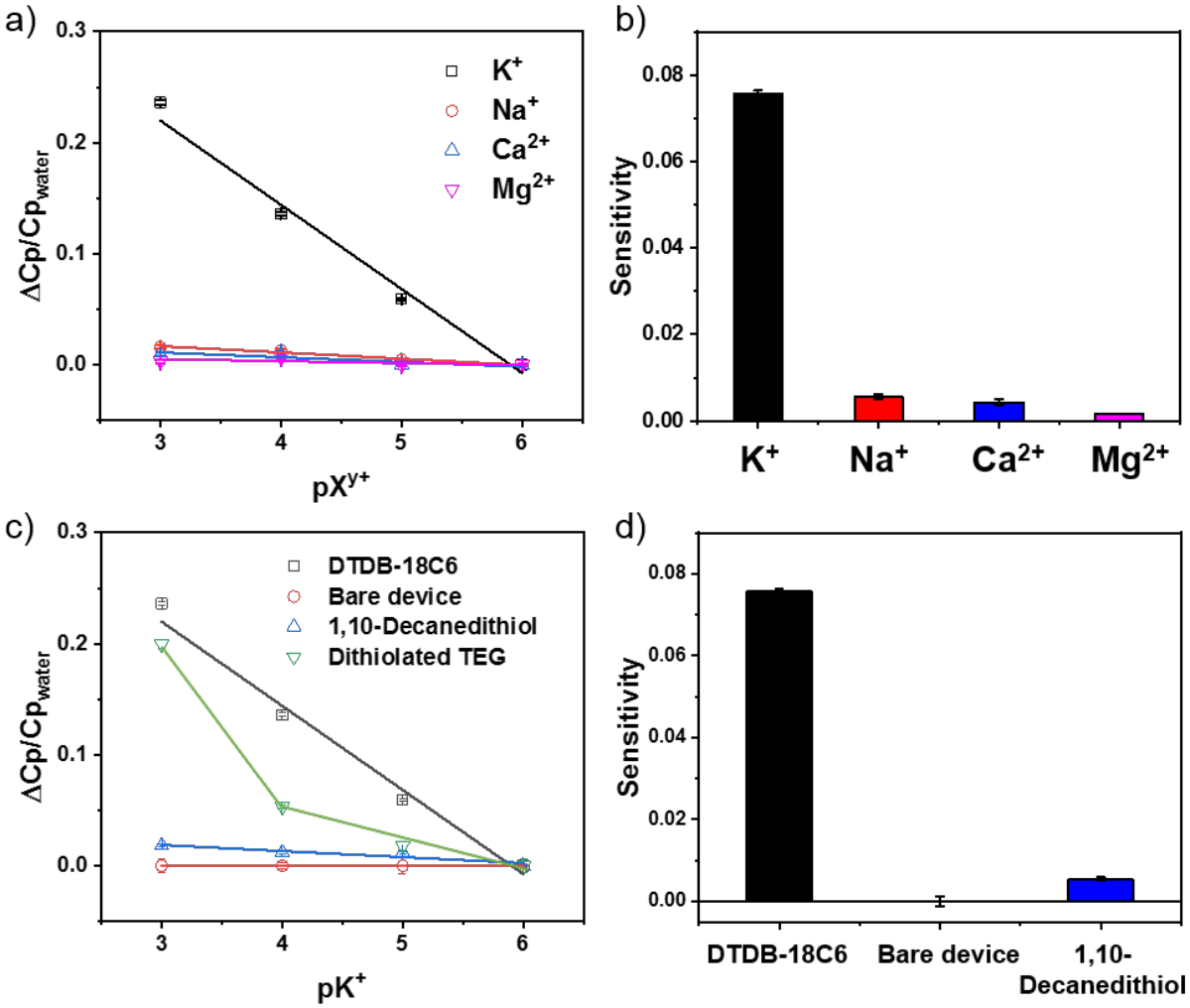

Figure 4: a) Normalized capacitance variation ($\Delta Cp/Cp_{water}$) and b) respective sensitivity of CRs based on AuNPs-DB18C6 networks towards diverse metal cations. c) Normalized capacitance response, and d) sensitivity to K^+ by using different molecular linkers for the network formation. Cp was recorded at 0.1 Hz.

2.5. Continuous Sensing Under Analyte Flow

Real-time monitoring of analytes continuously varying their concentration is a decisive characteristic in several chemical sensing applications.[36] Aiming to reach this high-demanding goal, a microfluidic cell has been designed to deliver small amounts (0.4 mL/min) of analyte on demand to the sensor surface. For this purpose, a new IDE layout has been designed to be accommodated in such a fluidic platform (**Figure 5a** and Figure S25). In addition to the

possibility to perform real-time measurements, different technological drawbacks can be avoided by using a microfluidic platform, e.g. no exposition of the device to adventitious contaminations from the environment, no solution evaporation during long-term analysis, drastic reduction of the sample volume, and standardization of the sample handling.

Real-time analyte monitoring has been performed in a way to verify both the CR sensitivity and the reversibility of its output signal (Cp). This means that two specular ramps of K^+ concentrations have been explored (i.e. increase from 10^{-6} to 10^{-3} M, and decrease from 10^{-3} to 10^{-6} M, with a pace of one decade) interspersed by a rinsing step in water before each K^+ concentration (**Figure 5b**). This experiment lasted 6000 s by using a constant solution flow equal to 0.4 mL/min; allowing us to record 10 consecutive measurements at each analyte concentration. Regarding the kinetics of complexation/release, the non-covalent interaction between K^+ and receptor is faster than the minimum Cp acquisition time (viz. 18 s). Upon water rinse, the device showed a perfect recovery of its basal signal, which hints to comparable kinetics for complexation and release. Additionally, no electrical degradation (RSD lower than 1.5% for any experimental point) or significant signal drift have been observed in the time scale of such experiments. Furthermore, the reversibility of K^+ detection has been successfully proved, with a sensitivity of (105 ± 8) x 10^{-3} pK^{-1} and (101 ± 8) x 10^{-3} pK^{-1} for both forward and backward ramps of K^+ concentrations, respectively.

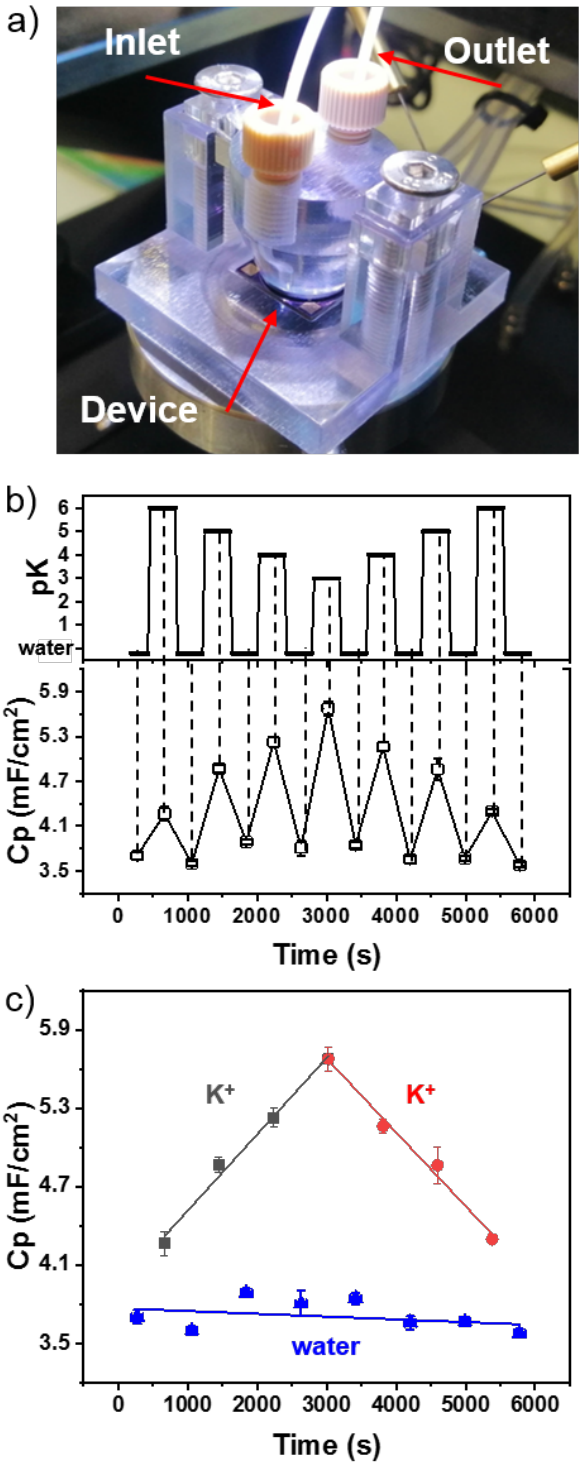

Figure 5: a) Picture of the microfluidic system, b) CR response under a flow of K^+ at different concentrations. The K^+ concentration was initially increased from 10^{-6} M to 10^{-3} M and then decreased from 10^{-3} M to 10^{-6} M, interspersed by a rising step in water before each K^+ concentration, c) calibration curve for the CR response with K^+ concentration increasing and

decreasing (red curves). The CR response in water is also shown (blue curve). Cp was recorded at 0.1 Hz.

2.6. K^+ Monitoring in Artificial Saliva

One of the main applications for POC K^+ sensors refers to the development of novel, non-invasive technologies for health monitoring.[37] For this purpose, the devised sensor should be able of detecting K^+ in a complex physiological media, for example, saliva – one of the most accessible bodily fluids, along with sweat – where variations of K^+ concentration can indicate the presence or the early stage of a disease in course, such as cystic fibrosis [38] Here, we have tested the performance of our CRs in artificial saliva as a proof-of-concept K^+ sensor for the development of future, non-invasive POC technologies for health monitoring.

Since the physiological content of K^+ in saliva varies within 3 mM and 20 mM, the CR calibration curve has been obtained by preparing K^+-spiked artificial saliva featuring a concentration between 0.5 and 50 mM (**Figure 6**) followed by a 1:100 in dilution in Milli Q water. The CR output signal has been recorded in static mode, namely by manually introducing every spiked aliquot of saliva onto the device surface. The linear regression of the device response yields a sensitivity equal to $(76 \pm 1)\ 10^{-3}\ pK^{-1}$ which is coherent to the previously reported benchmark test in aqueous K^+ solution. The CR performance (viz. sensitivity) is not jeopardized by the presence of interfering analytes such as Na^+, Mg^{2+}, Ca^{2+} or any other compound present in artificial saliva, confirming its efficiency as a selective K^+ sensor in complex media. We attribute the successful K^+ detection in both aqueous solution and saliva to the finely tuned characteristics of 3D networks based on AuNP-supramolecular receptors which provide reliable, fast, and recoverable signals that are ideal for CRs acting as transducers in POC sensing technologies.

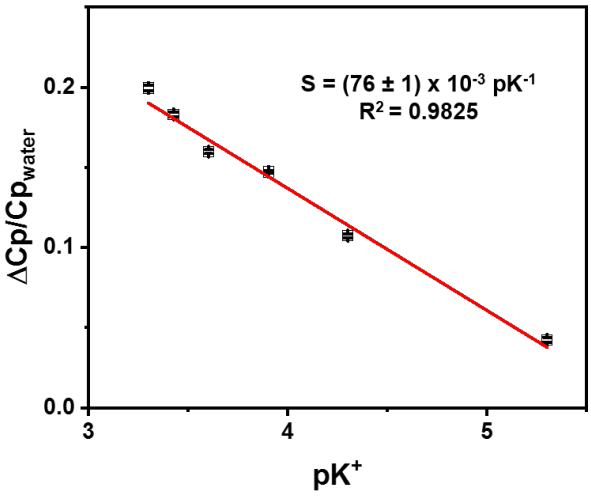

Figure 6: Normalized capacitance response of the CR against spiked K^+ in saliva samples. Spiked K^+ concentrations were varied between 0.5-50 mM. A dilution of 1:100 v/v is carried out previously to measurements in each case. Cp was recorded at 0.1 Hz.

3. Conclusion

In summary, we built up a novel and robust protocol for the assembly of 3D networks based on Au nanoparticles and dithiomethylene dibenzo-18-crown-6 ether supramolecular receptors a selective hosting material for CR sensing devices. A multiscale characterization allowed us to optimize the deposition method, the material's characteristics and the device architecture including the Au NP size, the adhesive layer, molecular receptor, the kinetics of the layer-by-layer assembly and the IDEs geometry. Such fine tuning made it possible to boost the CR performance. Our unprecedented technology showed outstanding figures of merits such as i) a robust shelf-life (viz. at least 45 days), ii) a high reversibility of the sensing signal, iii) a full compatibility with flow measurements for real-time K^+ monitoring, iv) a high sensitivity of (75 ± 1) x 10^{-3} pK^{-1} (linear range between 10^{-3} M and 10^{-6} M), and excellent selectivity (~ 13 times higher sensitivity) towards K^+ in the presence of diverse relevant interfering cations (Na^+, Ca^{2+} and Mg^{2+}), v) effective capability to detect K^+ cations in artificial saliva. Our findings provide unambiguous evidence that CRs bearing 3D networks precisely engineered with AuNPs and supramolecular receptors are ideal platforms for future developments of POC technologies for

health monitoring, where the detection of K^+ in saliva can be used for the non-invasive, early diagnostics of diseases.

4. Experimental Section

Materials: Chemicals for synthesis of (6, 7, 9, 10, 17, 18, 20, 21 -octahydrodibenzo [*b,k*] [1, 4, 7, 10, 13, 16] hexaoxacyclooctadecine-2,14-diyl) dimethanethiol were purchased from *Sigma Aldrich*, *TCI* and *Fluorochem* and were used as received. Solvents were purchased from *Fluorochem* and *Sigma Aldrich*, while deuterated solvents from *Eurisotop*. Poly(diallylmethylammonium chloride) solution (PDDA, 20 wt % in H_2O, average M_w 200,000−350,000 g/mol), sodium chloride (NaCl), tetra(ethylene glycol) (TEG) dithiol, anhydrous N,N-dimethylformamide (DMF), calcium chloride dihydrate ($CaCl_2$ $2H_2O$), sodium hydroxide (NaOH), potassium dihydrogen phosphate, sodium carboxymethyl cellulose (average Mw ~90,000 g/mol) and PD-sorbitol were supplied by Sigma-Aldrich. Trisodium citrate dihydrate, ethanol (EtOH) were supplied by Fisher. Hydrogen tetrachloroaurate(III) trihydrate, ($HAuCl_4 \cdot 3H_2O$, ACS, 99.99%), 3-(aminopropyl)triethoxysilane (APTES),1,10-Decanedithiol 99% were supplied by Alfa Aesar. Potassium chloride (KCl) was supplied by Fluka. Magnesium chloride ($MgCl_2$,) was supplied by Merk. Acetone and isopropanol were supplied by Carlo Erba reagents. SYLGARD™ 184 Silicone elastomer kit was purchased from the Dow chemical company. Milli-Q grade water was used in all preparations. The inert atmosphere was maintained by using nitrogen-filled balloons equipped with a syringe and needle to penetrate the silicon stoppers in the flask's necks. Additions of liquid reagents were performed using dried plastic or glass syringes. (6, 7, 9, 10, 17, 18, 20, 21 – octahydrodibenzo [b, k] [1, 4, 7, 10, 13, 16]hexaoxacyclooctadecine-2, 14 - diyl) dimethanol **1** was obtained according to literature.[39]

Synthesis of (6, 7, 9, 10, 17, 18, 20, 21 -octahydrodibenzo [b,k] [1, 4, 7, 10, 13, 16] hexaoxacyclooctadecine-2,14-diyl) dimethanethiol: The solution of (6, 7, 9, 10, 17, 18, 20, 21

– octahydrodibenzo [*b,k*] [1, 4, 7, 10, 13, 16] hexaoxacyclooctadecine-2, 14 - diyl) dimethanol **1** (1.10 g, 2.62 mmol) and Lawesson's reagent (2.22 g, 5.49 mmol) in toluene (70 mL) was heated at 110 °C under inert atmosphere for 48 h. The hot solvent was decanted from oily residue, the remaining material was refluxed in isopropanol (70 mL) for 30 min, then the solvent decanted again. The remaining solid material was dried in vacuum overnight to give crude polysulfide (935 mg). The crude polysulfide was dispersed in dry tetrahydrofuran (THF) (20 mL), the dispersion was degassed by bubbling nitrogen in sonicator for 20 min. and cooled down to -78 °C in dry ice and acetone bath. The suspension of $LiAlH_4$ (0.39 g, 10.3 mmol) in dry and degassed THF (20 ml) was added slowly to the cold dispersion of polysulfide and the reaction mixture left stirring in dry ice and acetone bath overnight letting it to warm up to room temperature (R.T.) slowly. After 12 h, the reaction mixture was cooled down to 0 °C and quenched by dropwise addition of saturated solution of NH_4Cl. The resulting reaction mixture was diluted with 10% HCl (50 mL) and washed with $CHCl_3$ (4 x 100 mL). The combined organic phases were dried over $MgSO_4$, filtered, and volatiles were removed in vacuum. The remaining solid residue was recrystallized from isopropanol to give *title* product 3 (350 mg, 37%) as colourless flakes; m.p.114-116 ^oC (from isopropanol); IR (ATR) ν (cm^{-1}): 2925 (w) and 2878 (w, Alk), 1592 (m), 1514 (s), 1472 (w), 1456 (m), 1429 (m), 1340 (w), 1334 (w), 1289 (m), 1261 (s), 1229 (s), 1167 (m), 1132 (s), 1081 (m), 1059 (m), 1043 (m), 989 (m), 958 (m), 931 (m), 903 (m), 856 (m), 834 (m), 800 (m), 784 (m), 740 (m), 684 (m), 665 (w), 654 (w), 644 (w), 630 (w), 603 (m), 588 (m), 585 (m), 570 (w), 563 (w), 556 (w), 536 (m), 533 (m), 527 (m), 521 (m), 517 (w), 510 (m), 502 (m); ^1H NMR (300 MHz, $CDCl_3$): δ = 6.88-6.72 (m, 6H, Ar*H*), 4.20-4.10 (m, 8H, 4CH_2), 4.05-3.96 (m, 8H, 4CH_2), 3.67 (d, J = 7.3 Hz, 4H, 2CH_2SH), 1.71 (t, J = 7.3 Hz, 2H, 2S*H*); ^{13}C NMR (75 MHz, $CDCl_3$): δ = 148.8 (s), 147.8 (s), 134.1 (s), 120.5 (d), 113.7 (d), 113.6 (d), 69.9 (*C*H_2), 69.0 (*C*H_2), 69.0 (*C*H_2), 68.9 (*C*H_2), 68.9 (*C*H_2), 28.7 (*C*H_2); HRMS (ESP): m/z [M+Na] calcd for ($C_{22}H_{28}O_6S_2Na$): 475.1225; found: 475.1227.

Synthesis of Au NPs: Citrate-stabilized Au NPs (diameter Ø ~12.5, 24 and, 40 nm) were synthesized following a seeded growth method previously reported by Bastús et al.[29]

Synthesis of 12.5 nm Au NPs: In brief, 150 mL of an aqueous solution of 2.2 mM trisodium citrate was heated to boiling under vigorous stirring. After 15 min, 1 mL of 25 mM $HAuCl_4$ in water was injected into the boiling solution. After 10 min, the colour of the solution changed from yellow to bright red, indicating the reaction is completed. The Au particles (~12.5 nm, ~3 10^{12} NPs/mL) are coated with negatively charged citrate ions and hence they are well-suspended in H_2O.

Synthesis of 24 and 40 nm Au NPs: The reaction mixture was cooled down to 90 °C after the synthesis of the 12.5 nm Au NPs in the same reaction vessel. Afterwards, a solution of 25 mM $HAuCl_{4(aq)}$ was added (1 mL). The reaction lasted 30 min, and it has been performed twice. Then, 55 mL was extracted from the reaction mixture, and subsequently, 53 mL of water and 2 mL of 60 mM sodium citrate (aqueous solution) were added. The resulting solution was then used as Au seeds for the following growing step. This process was repeated 3 or 7 times to yield 24 or 40 nm Au NPs respectively.

Electrode Fabrication: Test patterns containing four pairs of Au/Ti (100 nm/20 nm thick) interdigitated electrodes (IDEs) were produced by optical lithography on 15 mm × 15 mm glass substrates by Metrohm DropSens (Oviedo, Spain). Every chip has a total number of 36 fingers. The electrodes' width and their spacing are 10, 20, or 30 µm. The ratio between width and spacing is 1:1.

Bottom contact IDEs on Si/SiO_2 (Fraunhofer Institute IPMS, resistivity ρ_{Si} ~ 0.001 Ω·cm, oxide thickness t_{ox} = 90 nm) with 20 □m channel length were patterned by photolithography (AZ1505 photoresist and MIF726 developer, Micro Chemicals) using a Microtech LW405B laser writer. 5 nm Cr and 40 nm thick Au were thermally evaporated with Plassys MEB 300 following a lift-off process.

Fabrication of a Au NP monolayer: Glass test patterns were copiously rinsed in acetone and isopropanol for cleaning, followed by 20 min treatment by UV/ozone (NovaScan, Digital UV/Ozone System). Afterwards, the chips were immersed in 2 mL of the adhesive layer for a given time, rinsed, blown dry in N_2, and subsequently immersed in 2 mL of the previously purified Au NPs aqueous solution for 3 h. To remove the excess of reagents, 12.5 nm Au NPs were centrifuged at 8228 g for 30 min and redispersed in the same volume of water. Three different adhesive layers were evaluated: 1) APTES aqueous solution (1% v/v) for 30 min, 2) PDDA aqueous solution (1 mg mL^{-1}, 0.5 M NaCl) for 15 min, and 3) dithiolated TEG solution in EtOH (5 mM) for 48 h. The effect of the UV/ozone treatment and the purification of Au NPs were also studied. Finally, a PDMS reservoir was fabricated (silicon elastomer: curing agent 10:1, curing time 48 hours at R.T. in vacuum) and attached to the test pattern surface for the sensing experiments (Figure S11m Supporting information). The volume of the PDMS reservoir was ca.100-150 µL.

LbL Fabrication of Au NP-Networks: A glass chip containing a monolayer of Au NPs was placed inside a 5 mL vial, capped with a septum, and purged for 5 min with N_2. Dithiomethylene dibenzo-18-crown-6 ether solution (1mM) was prepared inside a glovebox in anhydrous DMF and in a septum capped vial. Afterwards, 100 µL of DTDB-18C6 solution was injected in the vial that contains the glass chip and let react for 20 min. Then, the septum was removed, and the substrate was immediately rinsed with water, blown dry in N_2, and 100 µL aqueous Au NPs solution was placed in the PDMS reservoir for 45 min. Later, the glass chip was rinsed with water, dried by an N_2 stream, and the following deposition of DTDB-18C6 was repeated. The alternated depositions of Au NPs and DTDB-18C6, which hereafter we denote together as 1 deposition step (DS), were repeated up to 11 times. Importantly, the last element of the depositions was always DTDB-18C6 molecules in order to remove all the citrate molecules from the surface of the Au NPs.

Experiments using test patterns with different channel lengths (10, 20, and 30 μm) and with Au NPs of different sizes (12.5, 24, and 40 nm Au NPs) were performed in order to optimize the sensing performance of the CRs.

As control experiments, different molecular linkers for the formation of Au NP networks have been tested, such as 1,10 undecanedithiol, and dithiolated TEG, whose backbones share the same molecular length of the DTDB-18C6. Networks and related devices were assembled following the optimized protocol employed for DTDB-18C8 receptors.

Electrical Measurements: The devices were electrically characterized by DC and AC electrical measurements. DC measurements were performed measuring the two-terminal device resistance at a constant bias of 100 mV. All DC electrical measurements were carried out in a probe station in ambient conditions by using a Keithley 2612B Source Meter unit.

AC measurements were performed by means of electrochemical impedance spectroscopy (EIS) employing a Metrohm Autolab PGSTAT204 potentiostat/galvanostat. The two-terminal EIS was recorded from 10^{-1} to 10^{5} Hz, swept from high to low frequencies, with a sine-wave voltage signal amplitude of 50 mV (root-mean-square, RMS). The device complex impedance (Z*) was converted into capacitance (Cp) using a simple parallel resistor-capacitor (RC) circuit (SI). Here, the measured Cp is expressed as the areal capacitance by taking into account the IDE dimensions.

Electrical Detection of K^+ ions in Static Mode: All the electrical characterizations were performed in wet state. 100 μL of KCl solutions (concentrations ranging from 10^{-1} to 10^{-9} M) were added into the PDMS reservoir placed on the surface of the devices (bare device, Au NP networks interconnected with DTDB-18C6, 1, 10 undecanedithiol or dithiolated TEG). The capacitance was recorded after 1 min of conditioning time. Control experiments with other cations, using NaCl, $CaCl_2$, and $MgCl_2$, were performed in an analogous way.

Microfluidic Cell Fabrication: The microfluidic was designed (Figure S25a) to satisfy the geometrical requirements of the silicon chip (Figure S25b) and the probe-station setup, where

the electrical measurements have been performed (Figure S25c). The microfluidic cell was manufactured by a Stratasys Objet30 3D printer using VeroClear resin and has an internal volume of ~12 µL. Aiming at getting a perfect sealing onto the silicon chip, the microfluidic cell was conceived to have a lower part which acts as a sample holder, where the silicon chip can be placed firmly (Figure S25c). The upper part is clamped to the lower one by two metallic screws, which allow controlling the pressure exerted onto the chip. The sealing is guaranteed by the presence of an o-ring upon the area where the IDEs are placed. The self-standing chip can be easily connected to the electrical probes and the tubes of the peristaltic pump (Figure S25c). This set-up has been used for the real-time monitoring of K^+ cations by impedance measurements.

Electrical Detection of K^+ Ions under Flow: The Si/SiO_2 chip was placed inside the microfluidic cell. A constant flow of KCl (0.4 mL min^{-1} of flow rate) was applied by using a Hei-FLOW-peristaltic pump and a Tygon tube (inner diameter 0.8 mm, wall thickness 1.6 mm). The capacitance response of the device to aqueous KCl solutions (concentrations ranging from 10^{-6} to 10^{-3} M) and water was recorded continuously for 1 h at 0.1 Hz.

Electrical Detection of K^+ Ions in Artificial Saliva: 500 mL of K^+-free artificial saliva were prepared using NaCl (1.02 g), NaH_2PO_4 (0.17g), $CaCl_2$ $2H_2O$ (0.148 g), $MgCl_2$ $6H_2O$ (0.025 g), sodium carboxymethyl cellulose (5 g) and sorbitol (15 g). The pH was adjusted to 6.75 with NaOH. KCl solutions (concentrations ranging from 0.5 to 50mM) were spiked in the saliva solutions. A dilution of 1:100 was performed by using Milli Q water and tested electrically as previously described.

Characterization: Thin layer chromatography (TLC) was conducted on pre-coated aluminum sheets with 0.20 mm *Merk Millipore* Silica gel 60 with fluorescent indicator F254. *Melting point* (mp): was measured on a *Gallenkamp* apparatus in open capillary tubes and have not been corrected. *Nuclear magnetic resonance:* (NMR) spectra were recorded on a Bruker Fourier 300 MHz spectrometer equipped with a dual (^{13}C, ^{1}H) probe. ^{1}H spectra were obtained at 300 MHz,

^{13}C spectra were obtained at 75 MHz NMR. All spectra were obtained at R.T. Chemical shifts were reported in ppm according to tetramethylsilane using the solvent residual signal as an internal reference ($CDCl_3$: δ_H = 7.26 ppm, δ_C = 77.16 ppm). Coupling constants (*J*) were given in Hz. Resonance multiplicity was described as *m* (multiplet), *d* (doublet) and *t* (triplet). ^{13}C spectra were acquired with a complete proton decoupling. The Attached Proton Test (APT) experiment was used to determine C-H multiplicities in carbon spectra and the peaks assigned as singlet (s) for quaternary and doublet (d) for tertiary carbon atoms. *Infrared spectrum* (IR) was recorded on a Shimadzu IR Affinity 1S FTIR spectrometer in ATR mode with a diamond mono-crystal. *Mass spectrometry:* High-resolution ESI mass spectrum (HRMS) was performed on a Waters LCT HR TOF mass spectrometer in the positive ion mode. The Visible-NIR extinction spectra of the Au NPs solutions and devices were recorded by using a JASCO V670 UV-Vis-NIR spectrophotometer. Optical images were acquired with an Olympus BX51 optical microscope. Scanning electron microscopy (SEM) imaging was conducted using FEI Quanta 250 FEG instrument operated in high vacuum mode (pressure in 10^{-4} Pa range), with accelerating voltages of 30 kV for the incident beam. ImageJ was used to calculate the Au NPs size and the coverage of the substrates from SEM images. X-ray photoelectron spectroscopy (XPS) analyses were carried out by using a Thermo Scientific K-alpha X-ray photoelectron spectrometer equipped with an aluminium X-ray source (energy 1.4866 keV). The spectra were recorded at a pressure of 10^{-8} mbar in the main chamber. The X-ray spot size was settled at 250 µm. Survey spectra were recorded as a result of 10 scans with a pass energy of 200.00 eV and a step size of 1 eV; high-resolution spectra were an average of 10 scans with a pass energy of 50.00 eV and a step size of 0.1 eV. Analysis of the XPS data was carried out using Avantage software. All the presented XPS spectra and subsequent data analysis were performed following the subtraction of the Shirley background from the region of interest. The Au4f and S2p XPS spectra were fitted using components with Gaussian/Lorentzian lineshapes and without full-

width-half-maximum (FWHM) values constrained. Neither the energy nor the relative area of the components was constrained.

Supporting Information
Supporting Information is available from the Wiley Online Library or from the author.

Acknowledgements

Device fabrication was carried out in part at the nanotechnology facility eFab (IPCMS, Strasbourg). The authors acknowledge funding from European Commission through the AMI project funded by the ERA-NET EuroNanoMed III programme, the European Union and the Agence Nationale de la Recherche (ANR) GA-ANR-17-ENM3-0001-01, the Marie Sklodowska-Curie projects ITN project BORGES (GA-813863), ERC project SUPRA2DMAT (GA-833707), ERC project Life-cycle (GA-757910), the MSCA-RISE project INFUSION (GA- 734834). the Agence Nationale de la Recherche through the Labex projects CSC (ANR-10-LABX-0026 CSC), and NIE (ANR-11-LABX-0058 NIE) within the Investissement d'Avenir program (ANR-10-120 IDEX-0002- 02), the International Center for Frontier Research in Chemistry (icFRC). DB and AB thank Cardiff University and University for financial support.

Received: ((will be filled in by the editorial staff))
Revised: ((will be filled in by the editorial staff))
Published online: ((will be filled in by the editorial staff))

References

[1] a) J. E. Brayden, M. T. Nelson, *Science* **1992**, 256, 532; b) D. A. Doyle, J. M. Cabral, R. A. Pfuetzner, A. Kuo, J. M. Gulbis, S. L. Cohen, B. T. Chait, R. MacKinnon, *Science* **1998**, 280, 69.
[2] S. A. Lanham-New, H. Lambert, L. Frassetto, *Advances in nutrition* **2012**, 3, 820.
[3] O. World Health, World Health Organization, Geneva 2009.
[4] P. M. Hald, W. B. Mason, in *Standard Methods of Clinical Chemistry*, Vol. 2 (Ed: D. Seligson), Elsevier **1958**, p. 165.
[5] M. d. G. A. Korn, D. S. S. d. Santos, B. Welz, M. G. R. Vale, A. P. Teixeira, D. d. C. Lima, S. L. C. Ferreira, *Talanta* **2007**, 73, 1.

[6] B.-S. Yu, L.-H. Nie, S.-Z. Yao, *Journal of Chromatography B: Biomedical Sciences and Applications* **1997**, 693, 43.
[7] M. Tounsi, M. Ben Braiek, H. Barhoumi, A. Baraket, M. Lee, N. Zine, A. Maaref, A. Errachid, *Materials Science and Engineering: C* **2016**, 61, 608.
[8] A. Verdian-Doghaei, M. R. Housaindokht, K. Abnous, *Analytical Biochemistry* **2014**, 466, 72.
[9] a) Y. Xie, *Sensors and Actuators B: Chemical* **2018**, 269, 22; b) J. Qiu, Y. Zhang, C. Dong, Y. Huang, L. Sun, H. Ruan, H. Wang, X. Li, A. Wu, *Sensors and Actuators B: Chemical* **2019**, 281, 783.
[10] S. Kumbhat, U. Singh, *Journal of Electroanalytical Chemistry* **2018**, 809, 31.
[11] a) H. Wohltjen, A. W. Snow, *Analytical Chemistry* **1998**, 70, 2856; b) F. J. Ibañez, F. P. Zamborini, *Small* **2012**, 8, 174.
[12] J. Liao, S. Blok, S. J. van der Molen, S. Diefenbach, A. W. Holleitner, C. Schönenberger, A. Vladyka, M. Calame, *Chemical Society Reviews* **2015**, 44, 999.
[13] N. Kang, F. Lin, W. Zhao, J. P. Lombardi, M. Almihdhar, K. Liu, S. Yan, J. Kim, J. Luo, B. S. Hsiao, M. Poliks, C.-J. Zhong, *ACS Sensors* **2016**, 1, 1060.
[14] Y.-C. Liu, C.-H. Hsu, B.-J. Lu, P.-Y. Lin, M.-L. Ho, *Dalton Transactions* **2018**, 47, 14799.
[15] M. S. Webster, J. S. Cooper, E. Chow, L. J. Hubble, A. Sosa-Pintos, L. Wieczorek, B. Raguse, *Sensors and Actuators B: Chemical* **2015**, 220, 895.
[16] a) K. Saha, S. S. Agasti, C. Kim, X. Li, V. M. Rotello, *Chemical Reviews* **2012**, 112, 2739; b) M. L. Tran, S. P. Centeno, J. A. Hutchison, H. Engelkamp, D. Liang, G. Van Tendeloo, B. F. Sels, J. Hofkens, H. Uji-i, *Journal of the American Chemical Society* **2008**, 130, 17240.
[17] J. Liao, L. Bernard, M. Langer, C. Schönenberger, M. Calame, *Advanced Materials* **2006**, 18, 2444.
[18] C. N. R. Rao, G. U. Kulkarni, P. J. Thomas, P. P. Edwards, *Chemical Society Reviews* **2000**, 29, 27.
[19] H. Wohltjen, W. R. Barger, A. W. Snow, N. L. Jarvis, *IEEE Transactions on Electron Devices* **1985**, 32, 1170.
[20] W. H. Steinecker, M. P. Rowe, E. T. Zellers, *Analytical Chemistry* **2007**, 79, 4977.
[21] B. Raguse, E. Chow, C. S. Barton, L. Wieczorek, *Analytical Chemistry* **2007**, 79, 7333.
[22] J. Mosquera, Y. Zhao, H.-J. Jang, N. Xie, C. Xu, N. A. Kotov, L. M. Liz-Marzán, *Advanced Functional Materials* **2020**, 30, 1902082.
[23] P. T. Bui, T. Nishino, *Physical Chemistry Chemical Physics* **2014**, 16, 5490.
[24] A. Foroushani, Y. Zhang, D. Li, M. Mathesh, H. Wang, F. Yan, C. J. Barrow, J. He, W. Yang, *Chemical Communications* **2015**, 51, 2921.
[25] E. S. Cho, J. Kim, B. Tejerina, T. M. Hermans, H. Jiang, H. Nakanishi, M. Yu, A. Z. Patashinski, S. C. Glotzer, F. Stellacci, B. A. Grzybowski, *Nature Materials* **2012**, 11, 978.
[26] R. Pinalli, A. Pedrini, E. Dalcanale, *Chemical Society Reviews* **2018**, 47, 7006.
[27] a) G. W Gokel, **1991**, DOI: 10.1039/9781788010917; b) L. F. Lindoy, *The Chemistry of Macrocyclic Ligand Complexes*, Cambridge University Press, Cambridge **1989**; c) D. J. C. Cram, Jane M **1997**, DOI: doi.org/10.1039/9781847550620; d) C. J. Pedersen, *Organic Syntheses* **1972**, 52, 66; e) G. W. D. GOKEL, H. Dupont, *Synthesis* **1976**, 3, 168; f) J.-C. Shen, W.-L. Jiang, W.-D. Guo, Q.-Y. Qi, D.-L. Ma, X. Lou, M. Shen, B. Hu, H.-B. Yang, X. Zhao, *Chemical Communications* **2020**, 56, 595; g) X.-D. Xu, J.-K. Ou-Yang, J. Zhang, Y.-Y. Zhang, H.-Y. Gong, Y. Yu, H.-B. Yang, *Tetrahedron* **2013**, 69, 1086.
[28] G. W. Gokel, W. M. Leevy, M. E. Weber, *Chemical Reviews* **2004**, 104, 2723.

[29] N. G. Bastús, J. Comenge, V. Puntes, *Langmuir* **2011**, 27, 11098.
[30] R. Furlan de Oliveira, P. A. Livio, V. Montes-García, S. Ippolito, M. Eredia, P. Fanjul-Bolado, M. B. González García, S. Casalini, P. Samorì, *Advanced Functional Materials* **2019**, 29, 1905375.
[31] a) B. Raguse, C. S. Barton, K.-H. Müller, E. Chow, L. Wieczorek, *The Journal of Physical Chemistry C* **2009**, 113, 15390; b) E. Chow, J. Herrmann, C. S. Barton, B. Raguse, L. Wieczorek, *Analytica Chimica Acta* **2009**, 632, 135; c) J. F. Fennell Jr., S. F. Liu, J. M. Azzarelli, J. G. Weis, S. Rochat, K. A. Mirica, J. B. Ravnsbæk, T. M. Swager, *Angewandte Chemie International Edition* **2016**, 55, 1266.
[32] T. P. Vello, R. F. de Oliveira, G. O. Silva, D. H. S. de Camargo, C. C. B. Bufon, *Scientific Reports* **2017**, 7, 43432.
[33] V. Spampinato, M. A. Parracino, R. La Spina, F. Rossi, G. Ceccone, *Frontiers in Chemistry* **2016**, 4.
[34] V. Montes-García, B. Gómez-González, D. Martínez-Solís, J. M. Taboada, N. Jiménez-Otero, J. de Uña-Álvarez, F. Obelleiro, L. García-Río, J. Pérez-Juste, I. Pastoriza-Santos, *ACS Applied Materials & Interfaces* **2017**, 9, 26372.
[35] R. M. Izatt, K. Pawlak, J. S. Bradshaw, R. L. Bruening, *Chemical Reviews* **1995**, 95, 2529.
[36] M. C. Frost, M. E. Meyerhoff, *Annual Review of Analytical Chemistry* **2015**, 8, 171.
[37] J. Kim, A. S. Campbell, B. E.-F. de Ávila, J. Wang, *Nature Biotechnology* **2019**, 37, 389.
[38] P. Kubáň, M. Greguš, E. Pokojová, J. Skřičková, F. Foret, *Journal of Chromatography A* **2014**, 1358, 293.
[39] M. J. van Eis, P. Seiler, L. A. Muslinkina, M. Badertscher, E. Pretsch, F. Diederich, R. J. Alvarado, L. Echegoyen, I. Pérez Núñez, *Helvetica Chimica Acta* **2002**, 85, 2009.